A Stabilized Multilevel Vector Finite-Element Solver for Time-Harmonic Electromagnetic Waves

Volker Hill, Ortwin Farle, and Romanus Dyczij-Edlinger, *Member, IEEE*

***Abstract*—An enhanced finite-element method (FEM) for the vector wave equation is presented. For improved speed and stability ranging from microwave frequencies down to the static limit, we propose a multilevel solver that uses a tree-gauged formulation on the coarsest mesh and a partially gauged scheme for the iterative cycle. Moreover, we have generalized the concept of hanging nodes to higher order $H(\mathrm{curl})$-conforming tetrahedral elements. The combination of hierarchical basis functions and the hanging variables framework yields great flexibility in placing degrees of freedom and provides a very attractive alternative to remeshing in an hp-adaptive context.**

***Index Terms*—Electromagnetic (EM) fields, finite-element methods (FEMs), wave propagation.**

I. Introduction

DURING the past decade, $H(\mathrm{curl})$ conforming basis functions have become the standard in finite-element methods (FEMs) for time-harmonic high-frequency problems. However, early field-based implementations were not well suited for iterative solvers. This difficulty was overcome by a vector potential formulation [1] that introduced an explicit basis for gradient fields. However, the price to be paid was almost twice the number of nonzeros in the system matrix. A subsequent development [2] exploited the properties of the discrete gradient operator to improve the memory and run time requirements, the partially gauged approach [3] helped minimize computational expenses for higher order basis functions, and the Schwarz-type solver [3] utilized multilevel ideas to improve numerical robustness for field domains that are electrically large. Meanwhile, the efficiency of iterative methods for high frequency problems was being further improved by the multigrid methods of [4] and [5], which employed gradient projections in their smoothers. Recently, a robust multigrid preconditioner for conjugate gradient (CG) type methods, which combines $\vec{E}$ field intergrid operators and ungauged vector potential relaxations, was proposed [6]. Optimized basis functions of higher order were presented in [7].

The present paper extends existing methods in two different directions. First, we do away with the lower frequency limit inherent in earlier approaches. With electric excitations, our method remains applicable even in the static limit. Based on the stabilized formulation, an efficient multilevel solver employing nested meshes and two polynomial levels is presented. Second, we utilize the interpolation properties of our FE spaces to extend the concept of hanging nodes [8] to higher order $H(\mathrm{curl})$ conforming elements. Since hanging variables allow finite elements of unequal refinement levels to be connected without violating continuity conditions, they are particularly useful in the context of nonuniform mesh refinement. While remeshing strategies or predefined splitting rules [9] may introduce elements of inferior quality, which must be removed in subsequent refinement steps, hanging variables keep the mesh hierarchy perfectly nested. Once the computational infrastructure for a multigrid scheme is in place, hanging variables can be implemented with very little effort.

Manuscript received June 18, 2002.

The authors are with the Department of Electrical Engineering, Lehrstuhl für Theoretische Elektrotechnik, Saarland University, Saarbrücken D-66123, Germany (e-mail: roman.edlinger@ieee.org).

Digital Object Identifier 10.1109/TMAG.2003.810379

II. Stabilized Potential Formulation

To motivate our approach, we shortly review existing formulations. Denoting the wavenumber, magnetic permeability, and electric permittivity by k, μ_r, and ϵ_r, the vector wave equation for the electrical field $\vec{E}$ is given by

$$\nabla \times \mu_r^{-1} \nabla \times \vec{E} - k^2 \varepsilon_r \vec{E} = 0. \tag{1}$$

The corresponding FE equation system can be written as

$$(S_{EE} - k^2 T_{EE}) \overline{x}_E = \overline{r}_E \tag{2}$$

where S_{EE} and T_{EE} stand for the stiffness and mass matrices, and $\overline{x}_E$ and $\overline{r}_E$ are the solution and right-hand side (RHS) vectors, respectively. Since (2) incorporates the gauge condition $\nabla \cdot \varepsilon_r \vec{E} = 0$ in wavenumber dependent form, the FE implementation breaks down in the static limit. At nonzero wavenumber, severe ill-conditioning may occur [1].

The simplified potential formulation [2], [6] is based on

$$\nabla \times \vec{A} = -jkc_0 \vec{B} \tag{3}$$

$$\vec{E} = \vec{A} + \nabla V \tag{4}$$

$$\nabla \times \mu_r^{-1} \nabla \times \vec{A} - k^2 \varepsilon_r (\vec{A} + \nabla V) = 0 \tag{5}$$

$$k^2 \nabla \cdot \varepsilon_r (\vec{A} + \nabla V) = 0 \tag{6}$$

where c_0 is the velocity of light. Note that (5) and (6) are linearly dependent. The key point with this method is that the corresponding FE equation system can be written as

$$\begin{bmatrix} S_{EE} - k^2 T_{EE} & -k^2 T_{EE} G \\ -k^2 G^T T_{EE} & -k^2 G^T T_{EE} G \end{bmatrix} \begin{bmatrix} \overline{x}_A \\ \overline{x}_V \end{bmatrix} = \begin{bmatrix} I \\ G^T \end{bmatrix} \overline{r}_E \tag{7}$$

where G is the discrete gradient operator, containing only two nonzero entries per row. By means of the identities [2] $G^T S_{EE} \equiv 0$ and $S_{EE} G \equiv 0$, we arrive at the final form

$$\begin{bmatrix} I \\ G^T \end{bmatrix} (S_{EE} - k^2 T_{EE}) \begin{bmatrix} I & G \end{bmatrix} \begin{bmatrix} \overline{x}_A \\ \overline{x}_V \end{bmatrix} = \begin{bmatrix} I \\ G^T \end{bmatrix} \overline{r}_E. \tag{8}$$

When iterative solvers are applied to the factorized system (8), memory and run time requirements become comparable to those of the field formulation, while the superior numerical properties of the potential formulation are preserved. There are two reasons why the method will fail when the wavenumber becomes small. The minor difficulty is with the factor k^2 in (6), which could be overcome by a suitable scaling routine. A more serious problem arises from the fact that, for efficiency, the system matrix is always stored as a single matrix $M_{EE} = S_{EE} - k^2 T_{EE}$. As the wavenumber approaches zero, the contribution from the mass matrix becomes arbitrarily small and, due the finite word length of digital computers, the identities

$$M_{EE}G \equiv (S_{EE} - k^2 T_{EE})G \equiv k^2 T_{EE}G \tag{9}$$

$$G^T M_{EE} \equiv G^T (S_{EE} - k^2 T_{EE}) \equiv k^2 G^T T_{EE} \tag{10}$$

fail to hold. Hence, (8) can no longer be used to recover the second row of (7). To overcome these deficiencies, we now set

$$\nabla \times \vec{A} = -jc_0 \vec{B} \tag{11}$$

$$\vec{E} = k\vec{A} - \nabla\phi \tag{12}$$

$$\nabla \times \mu^{-1} \nabla \times \vec{A} - \varepsilon(k^2 \vec{A} - k\nabla\phi) = 0 \tag{13}$$

$$\nabla \cdot \varepsilon(k\vec{A} - \nabla\phi) = 0 \tag{14}$$

and construct the FE matrices directly from the weak form

$$\int_\Omega \left[\nabla \times \vec{w}_A \cdot \mu_r^{-1} \nabla \times \vec{A} - \vec{w}_A \cdot \varepsilon_r (k^2 \vec{A} - k\nabla V)\right] d\Omega = -j\eta_0 \int_{\Gamma_H} \vec{w}_A \cdot \left(\overline{\vec{H} \times \hat{n}}\right) d\Gamma \tag{15}$$

$$\int_\Omega \nabla w_\phi \cdot \varepsilon_r (k\vec{A} - \nabla V)\, d\Omega = j\frac{\eta_0}{k} \int_{\Gamma_H} \nabla_T w_\phi \cdot \left(\overline{\vec{H} \times \hat{n}}\right) d\Gamma \tag{16}$$

where η_0 means the free space characteristic impedance, $\vec{w}_A$ and w_ϕ denote the vector and scalar FE weighting functions, $\hat{n}$ is the outer unit normal, and $\overline{\vec{H} \times \hat{n}}$ stands for the magnetic boundary values being imposed. Note that, in contrast to (6), the divergence constraint (14) does not vanish for $k = 0$. Moreover, we want to stress that the $1/k$ term on the RHS of (16) does not imply an instability of the formulation. Rather, it reflects the fact that with decreasing wavenumber, it becomes increasingly difficult to excite electric fields by magnetic boundary conditions.

III. Finite–Element Implementation

Our computer codes are based on tetrahedral elements. Let $\lambda_p (p = 0 \div 3)$ be the barycentric coordinates and single, double, and triple indexes denote vertices, edges, and facets, respectively. Then the second-order scalar basis functions read

$$n_p = \lambda_p \tag{17}$$

$$e_{kl} = 4\lambda_k \lambda_l \tag{18}$$

and a hierarchical basis [10] for the $H^1(\mathrm{curl})$ space is given by

$$\vec{w}_{kl} = \lambda_k \nabla\lambda_l - \lambda_l \nabla\lambda_k \tag{19}$$

$$\vec{g}_{kl} = 4\nabla(\lambda_k \lambda_l), \tag{20}$$

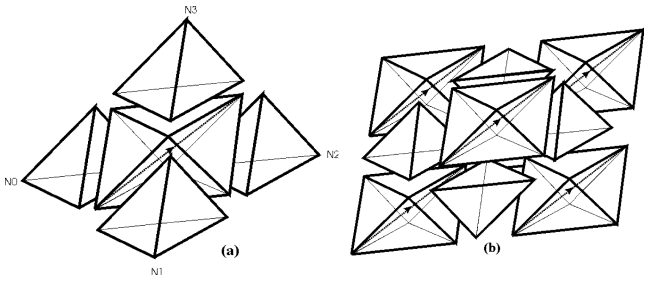

Fig. 1. Element subdivision. (a) Tetrahedron. (b) Octahedron.

$$\vec{f}_{ikl} = \lambda_i \vec{w}_{kl} \tag{21}$$

where $\vec{w}_{kl}$ represents the six-edge basis functions of the lowest order space $H^0(\mathrm{curl})$, augmented by one function per edge and two more functions $\vec{g}_{kl}$ per face. From (18) and (20), it is obvious that $\vec{g}_{kl} = \nabla e_{kl}$. By seeking $\vec{A}$ in the smaller space $H^0(\mathrm{curl}) \oplus span\vec{f}_{ikl}$, we impose a partial gauge which limits the ambiguity in the potentials to gauge transformations in $H^0(\mathrm{curl})$. At the same time, the computational overhead of the proposed formulation is significantly reduced. In practical applications, the number of nonzero matrix entries for the partially gauged $H^1(\mathrm{curl})$ scheme is just 25% higher than for the field formulation.

IV. Nested Tetrahedral Meshes

Our refinement scheme is inspired by the work in [8] and [9]. To derive its essential properties, we make use of auxiliary octahedral elements, which are never constructed in practice. As shown in Fig. 1(a), the coarse grid tetrahedron is split into four smaller tetrahedra which are similar to their parent plus one octahedron in the center. We define the "axis" of the octahedron by the diagonal that connects edge {01} to {23}. By splitting the octahedron along its axis, we obtain two pairs of congruent tetrahedra, which completes refinement level 1. To get to refinement level 2, we split the four outer tetrahedra as above. The center octahedron can be divided into six congruent octahedra of the same shape as their parent plus eight tetrahedra that are all similar to the coarse grid tetrahedron. Fig. 1(b) illustrates the situation. Again, we split each octahedron along its axis and obtain pairs of tetrahedra that are similar to those on level 1. Since none of the octahedra axes penetrates any boundaries of the level 1 tetrahedra, we have generated a valid splitting of the mesh on level 1. Hence, our refinement procedure results in only three classes of similar tetrahedra, implying that mesh quality will never deteriorate. The result itself is not new [9]. However, the above derivation provides us with a refinement strategy that does not require a single geometrical test once the orientation of the tetrahedron on the coarsest grid is fixed. In practice, we choose its orientation such that the axis of its child octahedron coincides with its shortest diagonal.

V. Intergrid Operators

Since our scalar FE basis is complete to second order, the coarse grid space is a proper subspace of the fine grid space, and the construction of the intergrid operator I_{2h}^h is straightforward [11]. We just give the block representation

$$\begin{bmatrix} \overline{c}_1 \\ \overline{c}_2 \end{bmatrix}_h = \begin{bmatrix} I_{11} & I_{12} \\ 0 & I_{22} \end{bmatrix} \begin{bmatrix} \overline{c}_1 \\ \overline{c}_2 \end{bmatrix}_{2h} \tag{22}$$

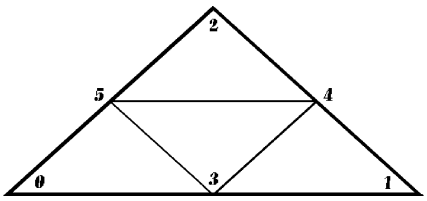

Fig. 2. Regular triangle subdivision and node numbering.

where $\overline{c}_1$ and $\overline{c}_2$ represent the coefficient vectors associated with first- and second-order basis functions, and the indexes h and $2h$ refer to the fine and coarse mesh, respectively.

On the other hand, the $H^1(\mathrm{curl})$ space is not second-order complete because the gradients of all homogeneous third-order polynomials are missing [12]. Nevertheless, it can be shown by construction that the subspace property also holds for the $H^1(\mathrm{curl})$ space. We now get

$$\begin{bmatrix} \overline{c}_e \\ \overline{c}_g \\ \overline{c}_f \end{bmatrix}_h = \begin{bmatrix} I_{ee} & I_{eg} & I_{ef} \\ 0 & I_{22} & I_{gf} \\ 0 & 0 & I_{ff} \end{bmatrix} \begin{bmatrix} \overline{c}_e \\ \overline{c}_g \\ \overline{c}_f \end{bmatrix}_{2h} \tag{23}$$

where $\overline{c}_e$, $\overline{c}_g$, and $\overline{c}_f$ are the coefficient vectors for edge, higher order gradient, and facial basis functions. Due to the large size of the intergrid operator (23) for the tetrahedron, we cannot give the coefficients in this paper but refer the interested reader to our web site [13]. However, to fix ideas, we present the underlying expansions of the coarse grid basis functions for the triangle shown in Fig. 2

$$\vec{w}_{01}^{\,2h} = \tfrac{1}{2}\,(\vec{w}_{03}^{\,h} + \vec{w}_{31}^{\,h}) + \tfrac{1}{4}\,(\vec{w}_{53}^{\,h} + \vec{w}_{34}^{\,h} + \vec{w}_{54}^{\,h}) \tag{24}$$

$$\vec{g}_{01}^{\,2h} = \tfrac{1}{4}\,(\vec{g}_{03}^{\,h} + \vec{g}_{31}^{\,h} + \vec{g}_{54}^{\,h}) + \vec{w}_{03}^{\,h} + \vec{w}_{53}^{\,h} + \vec{w}_{43}^{\,h} + \vec{w}_{13}^{\,h} \tag{25}$$

$$\vec{f}_{201}^{\,2h} = \tfrac{1}{8}\,\vec{w}_{54}^{\,h} + \tfrac{1}{16}\,(\vec{w}_{53}^{\,h} + \vec{w}_{34}^{\,h}) + \tfrac{1}{64}\,(\vec{g}_{35}^{\,h} - \vec{g}_{34}^{\,h}) + \tfrac{1}{8}\,(\vec{f}_{503}^{\,h} + \vec{f}_{354}^{\,h} + \vec{f}_{431}^{\,h} + \vec{f}_{254}^{\,h}). \tag{26}$$

Equation (26) reveals that the expansion of the coarse mesh function $\vec{f}^{\,2h}$ involves higher order gradients $\vec{g}^{\,2h}$ on the fine mesh which are not present in our FE representation of $\vec{A}$. By means of (12), the missing components can be expressed in terms of the scalar potential, which leads to the final, wavenumber-dependent form of the intergrid operator for the partially gauged potential formulation

$$\begin{bmatrix} \overline{c}_e \\ \overline{c}_f \\ \overline{c}_1 \\ \overline{c}_2 \end{bmatrix}_h = \begin{bmatrix} I_{ee} & I_{ef} & 0 & 0 \\ 0 & I_{ff} & 0 & 0 \\ 0 & 0 & I_{11} & I_{12} \\ 0 & -kI_{gf} & 0 & I_{22} \end{bmatrix} \begin{bmatrix} \overline{c}_e \\ \overline{c}_f \\ \overline{c}_1 \\ \overline{c}_2 \end{bmatrix}_{2h}. \tag{27}$$

VI. Multilevel Method

Our solver employs the CG method as an outer loop and uses a V-cycle as the preconditioner. The intergrid operator from (27) and its transverse are used to transfer residuals and corrections through the mesh hierarchy. Following [5] and [12], forward or back Gauss–Seidel iterations are performed at each pre- or post-smoothing stage, respectively. See [6] for a more sophisticated preconditioner. Thanks to the use of hierarchical basis functions, it is straight-forward to increase the polynomial degree of the approximation at any stage of mesh refinement. For improved numerical convergence, we employ the partially gauged approach of Section III whenever iterative methods are in use, i.e., on all the finer grids. However, on the coarsest mesh, we enforce uniqueness of the solution by imposing a tree gauge [14] on the $H^0(\mathrm{curl})$ variables, so that direct solvers can be applied without difficulties.

VII. Hanging Variables

Our strategy for inhomogeneous mesh refinement is as follows: Whenever an edge or face is to be refined, we subdivide all tetrahedra that have this entity in common. As a result, finite elements of different refinement levels get to touch at the outer boundary of the refined domain. To impose the proper continuity conditions, we restrict the fine mesh FE functions at the boundary such that they match those on the coarse mesh and express their associated coefficients $\overline{c}_B^{\,h}$ in terms of the coarse mesh coefficients $\overline{c}_B^{\,2h}$

$$\overline{c}_B^{\,h} = [I_B]\overline{c}_B^{\,2h}. \tag{28}$$

Let the triangle of Fig. 2 be located at the interface between coarse and fine mesh. Then the matrix entries of the boundary intergrid operator I_B are obtained from Section V as

$$c_{n3}^h = \tfrac{1}{2}\,(c_{n0}^{2h} + c_{n2}^{2h}) + c_{e01}^{2h}, \tag{29}$$

$$c_{e03}^h = c_{e31}^h = c_{e54}^h = \tfrac{1}{4}\,c_{e01}^{2h} \tag{30}$$

$$c_{w03}^h = \tfrac{1}{2}\,c_{w01}^{2h} + c_{g01}^{2h} \tag{31}$$

$$c_{g03}^h = \tfrac{1}{4}\,c_{g01}^{2h} \tag{32}$$

$$c_{w54}^h = \tfrac{1}{4}\,(c_{w01}^{2h} - c_{w12}^{2h} - c_{w20}^{2h}) + c_{g12}^{2h} - c_{g20}^{2h} + \tfrac{1}{8}\,c_{f201}^{2h} - \tfrac{1}{16}\,c_{f012}^{2h} \tag{33}$$

$$c_{g54}^h = \tfrac{1}{4}\,c_{g01}^{2h} + \tfrac{1}{64}\,c_{f201}^{2h} \tag{34}$$

$$c_{f254}^h = \tfrac{1}{8}\,c_{f201}^{2h}. \tag{35}$$

Given the assembled FE equation system for the fine region

$$\begin{bmatrix} M_{BB}^h & M_{BI}^h \\ M_{IB}^h & M_{II}^h \end{bmatrix} \begin{bmatrix} \overline{c}_B^{\,h} \\ \overline{c}_I^{\,h} \end{bmatrix} = \begin{bmatrix} \overline{r}_B^{\,h} \\ \overline{r}_I^{\,h} \end{bmatrix} \tag{36}$$

where indexes B and I denote quantities on the boundary and in the interior, respectively, the contribution to the global FE equation system is given by

$$\begin{bmatrix} I_B^T & 0 \\ 0 & I \end{bmatrix} \begin{bmatrix} M_{BB}^h & M_{BI}^h \\ M_{IB}^h & M_{II}^h \end{bmatrix} \begin{bmatrix} I_B & 0 \\ 0 & I \end{bmatrix} \begin{bmatrix} \overline{c}_B^{\,2h} \\ \overline{c}_I^{\,h} \end{bmatrix} = \begin{bmatrix} I_B^T & 0 \\ 0 & I \end{bmatrix} \begin{bmatrix} \overline{r}_B^{\,h} \\ \overline{r}_I^{\,h} \end{bmatrix}. \tag{37}$$

Since the matrix in (37) remains symmetric, and since couples neighboring elements on opposite sides of the fine mesh boundary only, the hanging variables framework preserves both symmetry and sparsity of the global FE matrix.

VIII. Numerical Examples

Throughout our tests, the number of Gauss–Seidel steps per smoothing stage is set to 3. Our first example is an air-filled

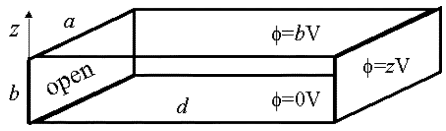

Fig. 3. Parallel plate waveguide. Dimensions: $a = 1$ m, $b = 0.5$ m, $d = 10$ m.

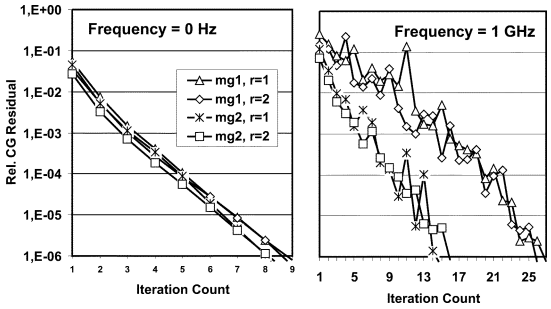

Fig. 4. Numerical convergence for the parallel plate waveguide example. The number of mesh refinement steps is given by the index r.

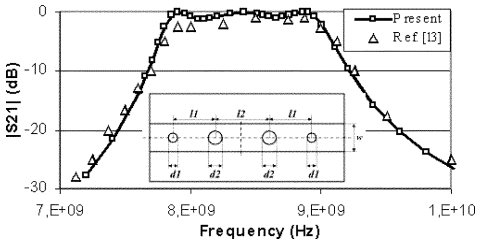

Fig. 5. Microstrip bandpass filter: $\epsilon_r = 2.43$, $d1 = 0.333$ mm, $d2 = 0.9323$ mm, $l1 = 10.42$ mm, $l2 = 11.15$ mm, $w = 3.79$ mm, substrate height $= 0.49$ mm.

parallel plate waveguide. As indicated in Fig. 3, the structure is excited by inhomogenous boundary conditions for the scalar potential. The coarsest mesh consists of 159 nodes and 715 edges. We compare two different refinement strategies: Multigrid scheme MG1 uses p-enrichment on the finest mesh, while the somewhat more expensive method MG2 employs $H^1(\mathrm{curl})$ elements from the coarsest level on. Fig. 4 shows that the rate on convergence does not depend on the number of refinement steps. Thanks to the richer function spaces at the coarser mesh levels, MG2 is much more effective in the high frequency case, whereas both methods perform equally well when the frequency is zero.

Our second example, the microstrip bandpass filter [15] shown in Fig. 5, has been chosen to demonstrate the versatility of our approach. We refine twice under the top conductor, once next to it, and keep the coarsest mesh in the air and outer substrate regions. We use $H^0(\mathrm{curl})$ elements in the air and $H^1(\mathrm{curl})$ elements everywhere else. The front view of one half of the structure can be seen in Fig. 6. The number of variables on the finest level is 276 278, and it takes at most 53 CG iterations to reach a relative residual of 1e-6. As shown in Fig. 5, our solutions are in very good agreement with measured results [15].

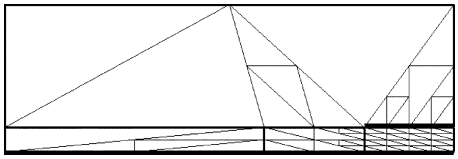

Fig. 6. Front view of one half of bandpass filter, showing hanging variables.

IX. Conclusion

We have presented a FEM for time-harmonic fields that extends down to the static limit, and we have proposed a hanging-variables framework that greatly improves the flexibility of our approach. Future work will focus on suitable error indicators to place degrees of freedom more efficiently.

References

[1] R. Dyczij-Edlinger and O. Biro, "A joint vector and scalar potential formulation for driven high frequency problems using hybrid edge and nodal finite elements," *IEEE Trans. Microwave Theory Tech.*, vol. 44, pp. 15–23, 1996.

[2] R. Dyczij-Edlinger, G. Peng, and J. F. Lee, "A fast vector-potential method using tangentially continuous vector finite elements," *IEEE Trans. Microwave Theory Tech.*, vol. 46, pp. 863–868, 1998.

[3] ——, "Efficient finite element solvers for the Maxwell equations in the frequency domain," *Comput. Methods Appl. Mech. Eng.*, vol. 169, pp. 297–309, 1999.

[4] R. Hiptmair, "Multigrid method for Maxwells equations," *SIAM J. Numer. Anal.*, vol. 36, pp. 204–225, 1998.

[5] R. Beck and R. Hiptmair, "Multilevel solution of the time-harmonic Maxwell equations based on edge elements," *Int. J. Numer. Methods Eng.*, vol. 45, pp. 901–920, 1999.

[6] Y. Zhu and A. C. Cangellaris, "Robust multigrid preconditioner for fast finite element modeling of microwave devices," *IEEE Microwave Wireless Components Lett.*, vol. 11, pp. 416–418, 2001.

[7] D. K. Sun, J. F. Lee, and Z. J. Cendes, "Construction of nearly orthogonal Nedelec bases for rapid convergence with multilevel preconditioned solvers," *SIAM J. Scientific Computing*, vol. 23, no. 4, pp. 1053–1076, 2001.

[8] J. P. Webb and S. McFee, "Nested tetrahedral finite elements for h-adaption," *IEEE Trans. Magn.*, vol. 33, pp. 1338–1341, 1999.

[9] F. Bornemann, B. Erdmann, and R. Kornhuber, "Adaptive multilevel methods in three space dimensions," Konrad Zuse Zentrum fuer Informationstechnik, Berlin, Germany, Rep. SC-92-14, 1992.

[10] J. P. Webb and B. Forghani, "Hierarchical scalar and vector tetrahedra," *IEEE Trans. Magn.*, vol. 29, pp. 1495–1498, 1993.

[11] W. L. Briggs, V. E. Henson, and S. F. McCormick, *A Multigrid Tutorial*, 2nd ed. Philadelphia, PA: SIAM, 2000.

[12] G. Peng, "Multigrid preconditioning in solving time-harmonic wave propagation problems using tangential vector finite elements," Ph.D. dissertation, Worcester Polytechnic Institute, Worcester, MA, 1997.

[13] [Online]. Available: http://www.lte.uni-saarland.de/publications/index.htm.

[14] R. Albanese and R. Rubinacci, "Solution of three dimensional eddy current problems by integral and differential methods," *IEEE Trans. Magn.*, vol. 24, pp. 98–101, 1988.

[15] K. L. Finch and N. G. Alexopoulos, "Shunt posts in microstrip transmission lines," *IEEE Trans. Microwave Theory Tech.*, vol. 38, pp. 1585–1594, 1990.